H ∞ active anti-roll bar control to prevent rollover of heavy vehicles: a robustness analysis

van Tan Vu, Olivier Sename, Luc Dugard, Peter Gáspár

H_∞ active anti-roll bar control to prevent rollover of heavy vehicles: a robustness analysis

Van-Tan Vu * **Olivier Sename** * **Luc Dugard** * **Peter Gaspar** **

* *Univ. Grenoble Alpes, GIPSA-lab, F-38402 Grenoble Cedex, France CNRS, GIPSA-lab, F-38402 Grenoble Cedex, France. E-mail: {Van-Tan.Vu, olivier.sename, luc.dugard}@gipsa-lab.grenoble-inp.fr*
** *Systems and Control Laboratory, Institute for Computer Science and Control, Hungarian Academy of Sciences, Kende u. 13-17, H-1111 Budapest, Hungary. E-mail: gaspar@sztaki.mta.hu*

Abstract: Rollover of heavy vehicle is an important road safety problem world-wide. Although rollovers are relatively rare events, they are usually deadly accidents when they occur. In order to improve roll stability, most of modern heavy vehicles are equipped with passive anti-roll bars to reduce roll motion during cornering or riding on uneven roads. This paper proposes an H_∞ approach to design active anti-roll bars using the yaw-roll model of a single unit heavy vehicle. The control signals are the torques generated by the actuators at the front and rear axles. Simulation results in both frequency and time domains are provided to compare two different cases: passive anti-roll bars and H_∞ active anti-roll bars. It is shown that the use of two H_∞ active (front and rear) anti-roll bars drastically improves the roll stability of the single unit heavy vehicle to prevent rollover.

Keywords: Vehicle dynamics, Active anti-roll bar control, Rollover, Roll stability, H_∞ control, μ-analysis.

1. INTRODUCTION

1.1 Context

The rollover is a very serious problem for heavy vehicle safety, which can result in large financial and environmental consequences. The aim of preventing rollovers is to provide the vehicle with an ability to resist overturning moments generated during cornering and lane changing to avoid obstacle.
In order to improve roll stability, most of modern heavy vehicles are equipped with **passive anti-roll bars** to reduce roll motion. The passive anti-roll bar force is a function of the difference between right and left suspensions deflections. The force is applied by the bar on each side of the vehicle so that the left force has the same magnitude but the opposite direction than the right one. The passive anti-roll bar has the advantages to reduce the body roll acceleration and roll angle during single wheel lifting and cornering maneuvers. However, the passive anti-roll bar also has drawbacks. During cornering maneuvers, anti-roll bar transfers the vertical forces of one side of suspension to the other one, creating therefore a moment against lateral force.
In order to overcome the drawbacks of the passive anti-roll bar systems, several schemes with possible active intervention into the vehicle dynamics have been proposed. One of these methods employs **active anti-roll bars**, that is, a pair of hydraulic actuators which generate a stabilizing moment to balance the overturning moment. Lateral acceleration makes vehicles with conventional passive suspension tilt out of corners. The center of the sprung mass shifts outboard of the vehicle centerline, which creates a destabilizing moment that reduces roll stability. The lateral load response is reduced by active anti-roll bars which generate a stabilizing moment to counterbalance the overturning moment in such a way that the control torque leans the vehicle into the corners (see Sampson and Cebon (2003), Gaspar et al. (2004)). Other methods can be used (active steering, electronic brake mechanism,...) but they are beyond the scope of this paper.
The disadvantage of the active anti-roll bars is that the maximum stabilizing moment is limited physically by the relative roll angle between the body and the axle (Sampson and Cebon (2002)).

1.2 Related works

Some of the control methods applied for active anti-roll bar control on heavy vehicle are briefly presented below:
a- Optimal control: Sampson *et al* (see Sampson and Cebon (1998), Sampson and Cebon (2002)) have proposed a state feedback controller which was designed by finding an optimal controller based on a linear quadratic regulator *(LQR)* for single unit and articulated heavy vehicles. They used the control torques acting between the axle groups and the sprung mass as the input control signal.
The *LQR* has been also applied to the integrated model including an electronic servo-valve hydraulic damper model and a yaw-roll model of a single unit heavy vehicle. The input control signal is the input current of the electronic servo-valve (Vu et al., 2016).
b- Neural network control: Boada et al. (2007) have proposed a reinforcement learning algorithm using neural networks to improve the roll stability for a single unit heavy vehicle. The input control signals are the torques at the axles. However this kind of approach is not suitable for embedded control.
c- Robust control *(LPV)***:** Gaspar *et al* (see Gaspar et al. (2005a), Gaspar et al. (2004) and Gaspar et al. (2005b)) have applied Linear Parameter Varying *(LPV)* for the active anti-roll bar combined with an active brake control on the single unit heavy vehicle. They also used a Fault Detection and Identification *(FDI)* filter, which identifies different actuator failures. The forward velocity is considered as the varying parameter.

1.3 Paper contribution

Based on the model presented in (Gaspar et al. (2004)), this paper proposes an H_∞ control method for active anti-roll bar, and focuses on the uncertainties due to the vehicle forward velocity and the sprung mass variations. Hence the following contributions are brought:

- We design a H_∞ robust controller for active anti-roll bar system on the single unit heavy vehicle. The aim is to maximize the roll stability to prevent rollover of heavy vehicles. The normalized load transfer and the limitation of the torque generated by actuators in various maneuver situations are considered.
- Performance analysis made in frequency domain shows that the H_∞ active anti-roll bar control drastically reduces the normalized load transfer compared to the passive anti-roll bar. It also shows that the H_∞ active anti-roll bar control is robust w.r.t. the forward velocity and the sprung mass variation. The robust stability analysis of the designed controller is performed using the μ- analysis method.
- In time domain, we use a double lane change as the heavy vehicle maneuver. The simulation results indicate that the *Root Mean Square (RMS)* of the H_∞ active anti-roll bar control have dropped from 15% to 50% compared to the passive anti-roll bar with all of the forward velocity considered in interval from $50Km/h$ to $110Km/h$.

The paper is organised as follows: Section 2 gives the model of a single unit heavy vehicle. Section 3 presents the design of the passive anti-roll bar. Section 4 gives the H_∞ robust control synthesis to prevent rollover of heavy vehicles. Section 5 illustrates the robustness analysis in the frequency domain using the μ- tool. Section 6 illustrates the simulations in time domain. Finally, some conclusions are drawn in section 7.

2. SINGLE UNIT HEAVY VEHICLE MODEL

Fig 1 illustrates the combined yaw-roll dynamics of the vehicle modelled by a three-body system, in which m_s is the sprung mass, m_{uf} the unsprung mass at the front including the front wheels and axle, and m_{ur} the unsprung mass at the rear with the rear wheels and axle. The parameters and variables of the yaw-roll model are shown in the table 1.

In the vehicle modelling, the differential equations of motion of the yaw-roll dynamics of the single unit vehicle, i.e. the lateral dynamics, the yaw moment, the roll moment of the sprung mass, the roll moment of the front and the rear unsprung masses, are formalized in the equations (1):

$$\begin{cases} mv(\dot\beta+\dot\psi)-m_s h\ddot\phi = F_{yf}+F_{yr} \\ -I_{xz}\ddot\phi + I_{zz}\ddot\psi = F_{yf}l_f - F_{yr}l_r \\ (I_{xx}+m_s h^2)\ddot\phi - I_{xz}\ddot\psi = m_s g h\phi + m_s v h(\dot\beta+\dot\psi) \\ \quad -k_f(\phi-\phi_{tf}) - b_f(\dot\phi-\dot\phi_{tf}) + M_{ARf} + U_f \\ \quad -k_r(\phi-\phi_{tr}) - b_r(\dot\phi-\dot\phi_{tr}) + M_{ARr} + U_r \\ -rF_{yf} = m_{uf}v(r-h_{uf})(\dot\beta+\dot\psi) + m_{uf}gh_{uf}.\phi_{tf} - k_{tf}\phi_{tf} \\ \quad +k_f(\phi-\phi_{tf}) + b_f(\dot\phi-\dot\phi_{tf}) + M_{ARf} + U_f \\ -rF_{yr} = m_{ur}v(r-h_{ur})(\dot\beta+\dot\psi) - m_{ur}gh_{ur}\phi_{tr} - k_{tr}\phi_{tr} \\ \quad +k_r(\phi-\phi_{tr}) + b_r(\dot\phi-\dot\phi_{tr}) + M_{ARr} + U_r \end{cases} \quad (1)$$

In (1) the lateral tire forces $F_{y;i}$ in the direction of velocity at the wheel ground contact points are modelled by a linear stiffness as:

$$\begin{cases} F_{yf} = \mu C_f \alpha_f \\ F_{yr} = \mu C_r \alpha_r \end{cases} \quad (2)$$

Table 1. Parameters of the yaw-roll model (see Gaspar et al. (2004))

Symbols	Description	Value	Unit
m_s	Sprung mass	12487	kg
$m_{u,f}$	Unsprung mass on the front axle	706	kg
$m_{u,r}$	Unsprung mass on the rear axle	1000	kg
m	The total vehicle mass	14193	kg
v	Forward velocity	-	$\frac{Km}{h}$
v_{wi}	Components of the forward velocity	-	$\frac{Km}{h}$
h	Height of CG of sprung mass from roll axis	1.15	m
$h_{u,i}$	Height of CG of unsprung mass from ground	0.53	m
r	Height of roll axis from ground	0.83	m
a_y	Lateral acceleration	-	$\frac{m}{s^2}$
β	Side-slip angle at center of mass	-	rad
ψ	Heading angle	-	rad
$\dot\psi$	Yaw rate	-	$\frac{rad}{s}$
α	Side slip angle	-	rad
ϕ	Sprung mass roll angle	-	rad
$\phi_{t,i}$	Unsprung mass roll angle	-	rad
δ_f	Steering angle	-	rad
u_i	Control current	-	A
C_f	Tire cornering stiffness on the front axle	582	$\frac{kN}{rad}$
C_r	Tire cornering stiffness on the rear axle	783	$\frac{kN}{rad}$
k_f	Suspension roll stiffness on the front axle	380	$\frac{kNm}{rad}$
k_r	Suspension roll stiffness on the rear axle	684	$\frac{kNm}{rad}$
b_f	Suspension roll damping on the front axle	100	$\frac{kN}{rad}$
b_r	Suspension roll damping on the rear axle	100	$\frac{kN}{rad}$
k_{tf}	Tire roll stiffness on the front axle	2060	$\frac{kNm}{rad}$
k_{tr}	Tire roll stiffness on the rear axle	3337	$\frac{kNm}{rad}$
I_{xx}	Roll moment of inertia of sprung mass	24201	kgm^2
I_{xz}	Yaw-roll product of inertial of sprung mass	4200	kgm^2
I_{zz}	Yaw moment of inertia of sprung mass	34917	kgm^2
l_f	Length of the front axle from the CG	1.95	m
l_r	Length of the rear axle from the CG	1.54	m
l_w	Half of the vehicle width	0.93	m
μ	Road adhesion coefficient	1	-

with tire side slip angles:

$$\begin{cases} \alpha_f = -\beta + \delta_f - \dfrac{l_f\dot\psi}{v} \\ \alpha_r = -\beta + \dfrac{l_r\dot\psi}{v} \end{cases} \quad (3)$$

Let us now detail how the moment M_{ARf} and M_{ARr} in (1) are computed. When the vertical displacements of the left and the right wheels differ, the passive anti-roll bar with a rotational stiffness k_{AO} creates an anti-roll moment, resulting in the anti-roll force F_{AU}, see Figure 2, acting on the unsprung mass as:

$$F_{AUl} = -F_{AUr} = k_{AU}(\Delta Z_{Ar} - \Delta Z_{Al}) \quad (4)$$

and the anti-roll force F_{AS} acting on the sprung mass is:

$$F_{ASl} = -F_{ASr} = F_{AUl}\frac{t_A}{t_B} = k_{AS}(\Delta Z_{Ar} - \Delta Z_{Al}) \quad (5)$$

where $\Delta Z_{Ar,l}$ are the displacements of the connection point between the anti-roll bars and the wheels, t_A is half the distance of the two suspensions, t_B is half the distance of the chassis, c is the length of the anti-roll bars's arm, k_{AU} and k_{AS} are the modified rotational stiffness corresponding to the unsprung and sprung mass, respectively:

$$k_{AU} = k_{AO}\frac{1}{c^2} \quad and \quad k_{AS} = k_{AO}\frac{t_A}{t_B c^2} \quad (6)$$

The moment of passive anti-roll bar impacts the unsprung and sprung masses at the front axle as follows:

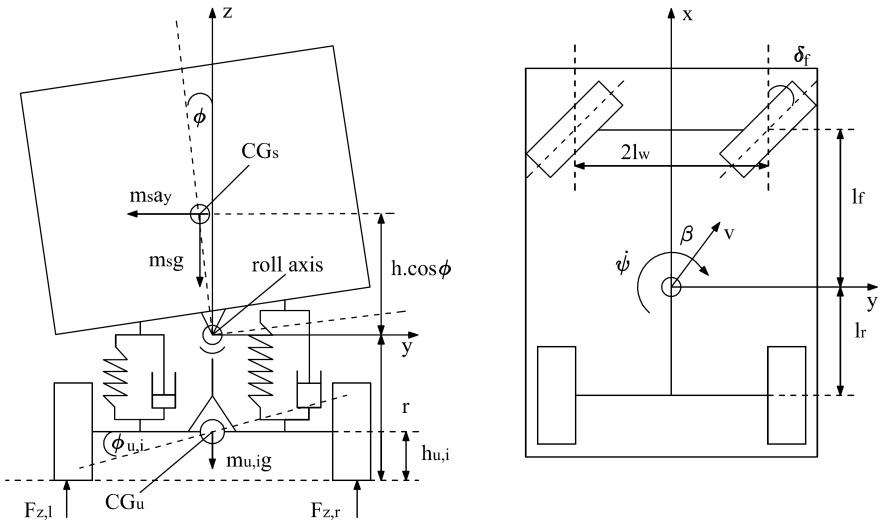

Fig. 1. Yaw-Roll model of single unit heavy vehicle (see Gaspar et al. (2004)).

$$M_{ARf} = 4k_{AOf}\frac{t_A t_B}{c^2}\phi - 4k_{AOf}\frac{t_A^2}{c^2}\phi_{uf} \tag{7}$$

The moment of passive anti-roll bar impacts the unsprung and sprung masses at the rear axle as follows:

$$M_{ARr} = 4k_{AOr}\frac{t_A t_B}{c^2}\phi - 4k_{AOr}\frac{t_A^2}{c^2}\phi_{ur} \tag{8}$$

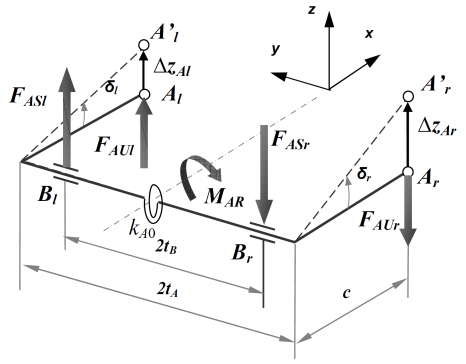

Fig. 2. Diagram of the passive anti-roll bars on the vehicles.

Using the previous equation, the single unit heavy vehicle is represented by the linear system in the state space form (9):

$$\begin{cases} \dot{x} = Ax + Bu \\ y = Cx \end{cases} \tag{9}$$

where the state vector:

$$x = \begin{bmatrix} \beta & \dot{\psi} & \phi & \dot{\phi} & \phi_{uf} & \phi_{ur} \end{bmatrix}^T$$

the input vector:

$$u = \begin{bmatrix} \delta_f & U_f & U_r \end{bmatrix}^T$$

and the output vector:

$$y = \begin{bmatrix} \beta & \dot{\psi} & \phi & \dot{\phi} & \phi_{uf} & \phi_{ur} \end{bmatrix}^T$$

Remark: Note that matrix A mainly depends on the forward velocity (V) and the sprung mass (m_s). The design of H_∞ controller will be done considering the nominal matrix A and the effect of uncertainties will be analysed in section 5.

3. DESIGN OF A PASSIVE ANTI-ROLL BAR

The design of an anti-roll bar actually aims at obtaining the required anti-roll stiffness k_{AO} that improves the vehicle stability and handling performances without exceeding the mechanical limitations of the bar material (Bharane et al. (2014) for general information about torsion bars and their manufacturing processing in *Spring Design Manual*). Anti-roll bars are special cases of torsion bars. Some useful formulae to calculate the torsional stiffness of anti-roll bars and deflection at the end point of the bar under a given loading, are provided in the manual. However, the formulations can only be applied to the bars with standard shapes (simple, torsion bar shaped anti-roll bars). The applicable geometry is shown in Figure 3.

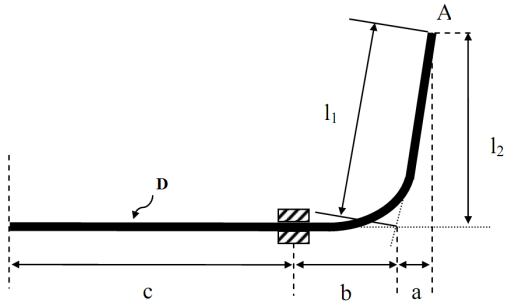

Fig. 3. Anti-roll bar geometry used in SAE Spring Design Manual.

The load P is applied at point A, inward to or outward from plane of the page. The roll stiffness of such a bar can be calculated as:

$$k_{AO} = \frac{PL^2}{2f_A} \tag{10}$$

with f_A - Deflection of point A:

$$f_A = \frac{P}{3EI}[l_1^3 - a^3 + \frac{L}{2}(a+b)^2 + 4l_2^2(b+c)] \tag{11}$$

L - Half track length of anti-roll bar:

$$L = a + b + c \tag{12}$$

and I - Moment of inertia of anti-roll bar:

$$I = \pi\frac{D^4}{64} \tag{13}$$

where D is the outer diameter and E the young's modulus of material.
The material of anti-roll bar is issued from *AISI 1065*, $E = 206000MPa$ (see Bharane et al. (2014)). The outer diameter of the anti-roll bar on the front axle $D_f = 32mm$ (Vu et al., 2016), the torsional stiffness of the anti-roll bar at the front axle is:

$$k_{AOf} = 10730 \quad (\frac{Nm}{rad})$$

The outer diameter of the anti-roll bar on the rear axle $D_r = 34mm$ (Vu et al., 2016), the torsional stiffness of the anti-roll bar at the rear axle is:

$$k_{AOr} = 15480 \quad (\frac{Nm}{rad})$$

4. H_∞ ROBUST CONTROL SYNTHESIS TO PREVENT ROLLOVER OF HEAVY VEHICLES

4.1 Control objective, problem statement

The objective of the active anti-roll bar control system is to maximize the roll stability of the vehicle. The rollover is caused by the high lateral inertial force generated by lateral acceleration. If the position of the center of gravity is high or the forward velocity of the vehicle is larger than allowed at a given steering angle, the resulting lateral acceleration is also large and might initiate a rollover. An imminent rollover can be detected if the calculated normalized load transfer reaches 1 (or -1), as explained below.
First, the lateral load transfer can be given by:

$$\Delta F_z = \frac{k_u \phi_u}{l_w} \tag{14}$$

where k_u is the stiffness of tire, ϕ_u the roll angle of the unsprung mass and l_w the half of vehicle's width. Then, the lateral load transfer can be normalized w.r.t. the total axle load F_z as follows:

$$R = \frac{\Delta F_z}{F_z} \tag{15}$$

The normalized load transfer R value corresponds to the largest possible load transfer. When $R = \pm 1$, the inner wheel in the bend lifts off.
The roll stability is achieved by limiting the normalized load transfer within the levels corresponding to wheel lift-off. Specifically, the load transfer can be minimized to increase the inward lean of the vehicle. The center of mass shifts laterally from the nominal center line of the vehicle to provide a stabilizing effect. While attempting to minimize the load transfer, it is also necessary to constrain the roll angles between the sprung and unsprung masses ($\phi - \phi_u$) so that they stay within the limits of the suspension travel ($(7 - 8deg)$ see Gaspar et al. (2004)).
The performance characteristic which is of most interest when designing the active anti-roll bar, is then the normalized load transfer. The chosen control objective is to minimize the effect of the steering angle δ on the normalized load transfer R, in the H_∞ framework. As explained later, the limitation of the torques $U_{f,r}$ generated by actuators is crucial for practice implementation.

4.2 Background on H_∞ control

The interested reader may refer to (Skogestad and Postlethwaite, 2001), (Scherer and Weiland, 2005) for further explanations on H_∞ control design.
The H_∞ control problem is formulated according to the generalized control structure shown in Fig 4.

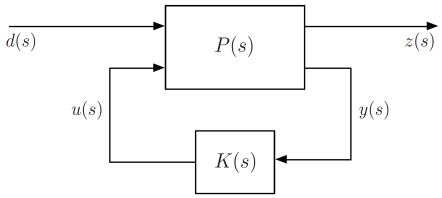

Fig. 4. Generalized control structure.

with P partitioned as

$$\begin{bmatrix} z \\ y \end{bmatrix} = \begin{bmatrix} P_{11}(s) & P_{12}(s) \\ P_{21}(s) & P_{22}(s) \end{bmatrix} \begin{bmatrix} d \\ u \end{bmatrix} \tag{16}$$

and

$$u = K(s).y \tag{17}$$

which yields

$$\frac{z}{d} = \mathcal{F}_l(P,K) := [P_{11} + P_{12}K[I - P_{22}K]^{-1}P_{21}] \tag{18}$$

The aim is to design a controller K that reduces the signal transmission path from disturbances d to performance outputs z and also stabilizes the closed-loop system. This problem aims at finding K which minimizes γ such that

$$\|\mathcal{F}_l(P,K)\|_\infty < \gamma \tag{19}$$

By minimizing a suitably weighted version of (19) the control aim is achieved, as presented below.

4.3 H_∞ control synthesis for the active anti-roll bar of the single unit heavy vehicle model

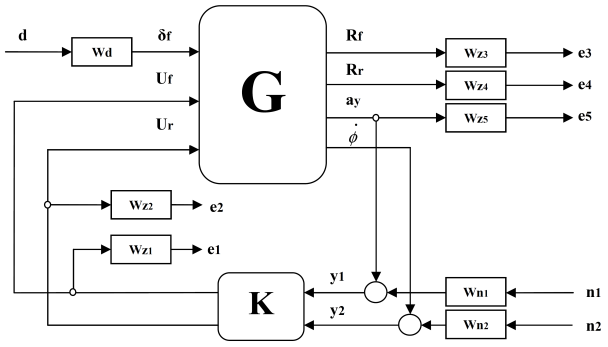

Fig. 5. $G-K$ control structure of H_∞ active anti-roll bar control.

In this section, the H_∞ control design is presented for the active anti-roll bar system on single unit heavy vehicle. Consider the closed-loop system in Fig 5, which includes the feedback structure of the nominal model G, the controller K and weighting functions that are presented below. In the diagram, U_f and U_r are the control inputs, y_1 and y_2 are the measured outputs, n_1 and n_2 are the measurement noises. δ_f is the steering angle as a disturbance signal, which is set by the driver. The e_1, e_2, e_3, e_4 and e_5 represent the performance outputs.
According to Fig 5 the concatenation of the linear model (9) with performance weighting functions lead to the state space representation of $P(s)$:

$$\begin{bmatrix} \dot{X} \\ Z \\ Y \end{bmatrix} = \begin{bmatrix} A & B_1 & B_2 \\ C_1 & D_{11} & D_{12} \\ C_2 & D_{21} & D_{22} \end{bmatrix} \begin{bmatrix} X \\ W \\ U \end{bmatrix} \tag{20}$$

with the exogenous input (disturbance):

$$W = \begin{bmatrix} d & n_1 & n_2 \end{bmatrix}$$

the control input:

$$U = \left[U_f \;\; U_r \right]^T$$

where U_f is the torque at the front axle, U_r is the torque at the rear axle.
the performance output vector:

$$Z = \left[e_1 \;\; e_2 \;\; e_3 \;\; e_4 \;\; e_5 \right]^T$$

the measured output vector:

$$Y = \left[a_y \;\; \dot{\phi} \right]^T$$

and A, B_1, B_2, C_1, D_{11}, D_{12}, C_2, D_{21}, D_{22} are model matrices of appropriate dimensions.
In H_∞ control the selection of the weighting functions is a key step that is to be handled using the knowledge of the engineers concerning the system behavior and characteristics. The weighting functions of Fig 5 are given here after.
The input scaling weight W_d normalizes the steering angle to the maximum expected command and is selected as follows:

$$W_d = \pi/180$$

This value corresponds to a 1^0 steering angle command.
The weighting functions W_{n1} and W_{n2} are selected as:

$$W_{n1} = W_{n2} = 0.01$$

which accounts for small sensor noise models in the control design. The noise weights are chosen $0.01(m/s^2)$ for the lateral acceleration and $0.01(^0/sec)$ for the derivative of roll angle $\dot{\phi}$ (see (Gaspar et al., 2004)). Other low pass filters could be selected.
The weighting functions W_{zi} represent the performance outputs (W_{z1}, W_{z2}, W_{z3}, W_{z4} and W_{z5}). The purpose of the weighting functions is to keep small the control inputs, normalized load transfers and the lateral acceleration over the desired frequency range. The weighting functions chosen for performance outputs can be considered as penalty functions, that is, weights should be large in the frequency range where small signals are desired and small where larger performance outputs can be tolerated.
The weighting functions W_{z1} and W_{z2} are chosen as:

$$W_{z1} = 1/1.5x10^5, \quad W_{z2} = 1/2x10^5$$

which correspond to the front and rear control torques generated by active anti-roll bars.
The weighting functions W_{z3} and W_{z4} are selected as:

$$W_{z3} = W_{z4} = 1$$

which means that the maximal gain of the normalized load transfers can be 1 in the frequency domain for front and rear axles.
The weighting function W_{z5} is selected as:

$$W_{z5} = \frac{(s/2000 + 50)}{(s/0.01 + 0.01)} \tag{21}$$

Here, the weighting function W_{z5} corresponds to a design that avoids the rollover situation with the bandwidth of the driver in frequency range up to more than $4rad/s$. This weighting function will minimize directly the lateral acceleration when it reaches the critical value to avoid the rollover.

4.4 Frequency domain analysis with nominal value

The limited bandwidth of the driver must be considered up to $4rad/s$ to identify any resonances in the response that may be excited by the driver (see Gaspar et al. (2004) and Sampson (2000)). Therefore, it is necessary to consider the behavior of the heavy vehicle in a wider frequency range. In this section, the frequency response of heavy vehicle is shown in the nominal parameters case.
The nominal parameters of single unit heavy vehicle considered include the sprung mass $m_s = 12487kg$, the forward velocity V at $70Km/h$ and the road adhesion coefficient $\mu = 1$. The frequency responses of the single unit heavy vehicle are shown in Fig 6.
Fig 6*a* shows the normalized load transfer at the front axle R_f due to steering angle δ_f. It shows that the H_∞ active anti-roll bar controller reduces the normalized load transfer (about $3dB$) in frequency range up to $7.0rad/s$ compared to the passive anti-roll bar. Fig 6*b* shows the normalized load transfer at the rear axle R_r. It indicate that the H_∞ active anti-roll bar controller reduces the normalized load transfer at the rear axle (about $4.5dB$) throughout the main frequency range. As a consequence, the H_∞ active anti-roll bar can improve the roll stability to prevent rollover.
Fig 6*a*,*b* also indicate that the normalized load transfers build up more quickly at the rear axle than at the front axle with the cases of the passive anti-roll bar as well as the H_∞ active anti-roll bar. This is consistent with the previous results (see (Sampson, 2000)).
The simulation results in Fig 6*a*,*b* fulfil the main objective of designing H_∞ active anti-roll bar control system which is to minimize the normalized load transfer to prevent rollover of heavy vehicle.
Fig 6*c*,*d* show the control inputs of the H_∞ active anti-roll bar which are the torque at the front (U_f) and the rear axle (U_r). It indicates that the torque at the rear axle is always greater than that of front axle about $5dB$ throughout the main frequency range. This ensures that the normalised load transfer at rear axle is more minimized than that at the front axle. This explains why the normalised load transfers at the front and rear axles for the passive anti-roll bar are $23dB$ and $25dB$, respectively. Meanwhile, the normalised load transfers at the front and rear axles for the H_∞ active anti-roll bar control equal approximately $20dB$.

5. ROBUSTNESS ANALYSIS IN THE FREQUENCY DOMAIN USING THE μ- TOOL

5.1 Robust stability and performance analysis

A control system is robust if it is insensitive to differences between the actual real system and the model used to design the controller. Let us recall that, in addition to nominal stability and performance, the objectives of any control system include:
Robust Stability (RS). The system is stable for all perturbed plants around the nominal model up to the worst-case model uncertainty.
Robust Performance (RP). The system satisfies the performance specifications for all perturbed plants around the nominal model up to the worst-case model uncertainty.
The current application is concerned by parametric uncertainties. In particular, the forward velocity and the sprung mass are assumed to be badly known. In the considered *yaw-roll* model (1), the forward velocity is the most varying parameter. The other parameters variations come from the industrial manufacturing only. The uncertainties are therefore represented as:

$$\begin{array}{lll} \overline{V} & = V(1 + p_V\delta_V), & p_V = 57.14\%,\ \delta_V \in [-1;1] \\ \overline{m_s} & = m_s(1 + p_{m_s}\delta_{m_s}), & p_{m_s} = 30\%, \quad \delta_{m_s} \in [-1;1] \end{array}$$

Using ad hoc *LFT* representations of the parametric uncertainties, we can pull out the perturbations in a diagonal block as: $\Delta_r = \mathrm{diag}\{\delta_V I_V, \delta_{m_s} I_{ms}\}$.

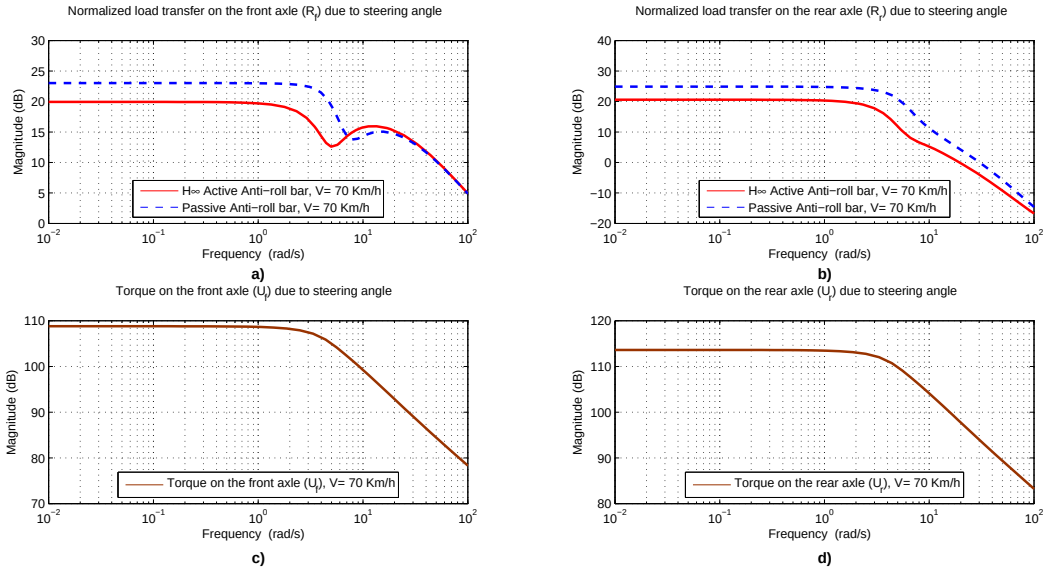

Fig. 6. Frequency responses of the normalized load transfer ($R_{f,r}$) and the torque ($U_{f,r}$) due to steering angle.

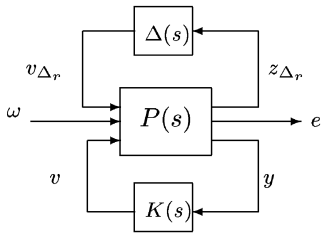

Fig. 7. General control configuration with uncertainties.

A- Background on robust stability

The starting point of the robustness analysis is the block-diagonal representation of the uncertainties set:

$\underline{\Delta} = \{\text{diag}\{\Delta_1, \cdots, \Delta_q, \delta_1 I_{r_1}, \cdots, \delta_r I_{r_r}, \epsilon_1 I_{c_1}, \cdots, \epsilon_c I_{c_c}\} \in \mathbb{C}^{k \times k}, \quad \Delta_i \in \mathbb{C}^{k_i \times k_i}, \quad \delta_i \in \mathbb{R}, \quad \epsilon_i \in \mathbb{C}\}$.

where $\Delta_i(s), i = 1, \ldots, q$, represent full block complex uncertainties, $\delta_i(s), i = 1, \ldots, r$, real parametric uncertainties, and $\epsilon_i(s), i = 1, \ldots, c$, complex parametric uncertainties.

Taking into account the uncertainties leads to the following General Control Configuration given in Fig 7, where $\Delta \in \underline{\Delta}$. Here, only real parametric uncertainties (Δ_r) are considered for *RS* analysis. *RP* analysis also needs a fictive full block complex uncertainty, as shown in Fig 8.

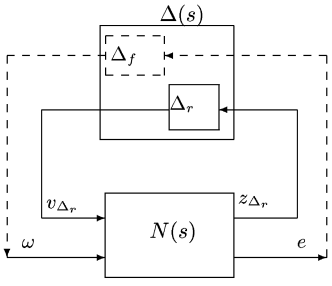

Fig. 8. $N\Delta$ structure.

where $N(s) = \begin{bmatrix} N_{11}(s) & N_{12}(s) \\ N_{21}(s) & N_{22}(s) \end{bmatrix}$, and the closed-loop transfer matrix is:

$$T_{ew}(s) = N_{22}(s) + N_{21}(s)\Delta(s)(I - N_{11}(s))^{-1}N_{12}(s) \qquad (22)$$

Note that in (22), $N_{22}(s) = N_{ew}$ is the nominal closed-loop transfer matrix. If it is stable, the unstability in (22) may only come from $(I - N_{11}(s))^{-1}$.

As we consider structured uncertainties, a μ-analysis is used for the *RS* and *RP* analysis. First the structured singular value is defined as:

$\mu_{\underline{\Delta}}(M)^{-1} := \min\{\overline{\sigma}(\Delta) : \Delta \in \underline{\Delta}, \det(I - \Delta M) \neq 0\}$.

For *RS*, we determine how large Δ (in the sense of H_∞) can be without destabilizing the feedback system. From (22), the feedback system becomes unstable if $det(I - N_{11}(s)) = 0$ for some $s \in \mathbb{C}, \Re(s) \geq 0$. The following theorem is used.

Theorem 1. (Skogestad and Postlethwaite, 2001) Assume that the nominal system N_{ew} and the perturbations Δ are stable. Then the feedback system is stable for all allowed perturbations Δ such that $\|\Delta(s)\|_\infty < 1/\beta$ if and only if $\forall \omega \in \mathbb{R}, \ \mu_{\underline{\Delta}}(N_{11}(j\omega)) \leq \beta$.

Assuming nominal stability, *RS* and *RP* analysis for structured uncertainties are therefore such that:

$$\text{RS} \Leftrightarrow \mu_{\Delta_r}(N_{11}) < 1, \ \forall \omega \qquad (23)$$

$$\text{RP} \Leftrightarrow \mu_{\Delta}(N) < 1, \ \forall \omega, \ \Delta = \begin{bmatrix} \Delta_f & 0 \\ 0 & \Delta_r \end{bmatrix} \qquad (24)$$

Finally, let us remark that the structured singular value cannot be explicitly determined. The method consists then in calculating an upper bound and a lower bound, as close as possible to μ.

B- Robust stability for H_∞ active anti-roll bar control

Apply the theorem 1, an upper bound of μ for *RS* and *RP* is given in Fig 9 and Fig 10. As $\mu_{\Delta_r}(N_{11}) \leq 0.6023$, *RS* is satisfied. Hence the H_∞ controller keeps stability for the considered uncertainties. Moreover, this means that the closed-loop system remains stable for larger uncertainties,i.e.:

$V = 70Km/h \pm (57.14/0.6023)\% = 70Km/h \pm 94.87\%$

$m_s = 12487kg \pm (30/0.6023)\% = 12487kg \pm 49.81\%$

On the other hand, as $\mu_{\Delta}(N) < 1$, we can conclude that the Robust Performance is satisfied in this uncertainty case.

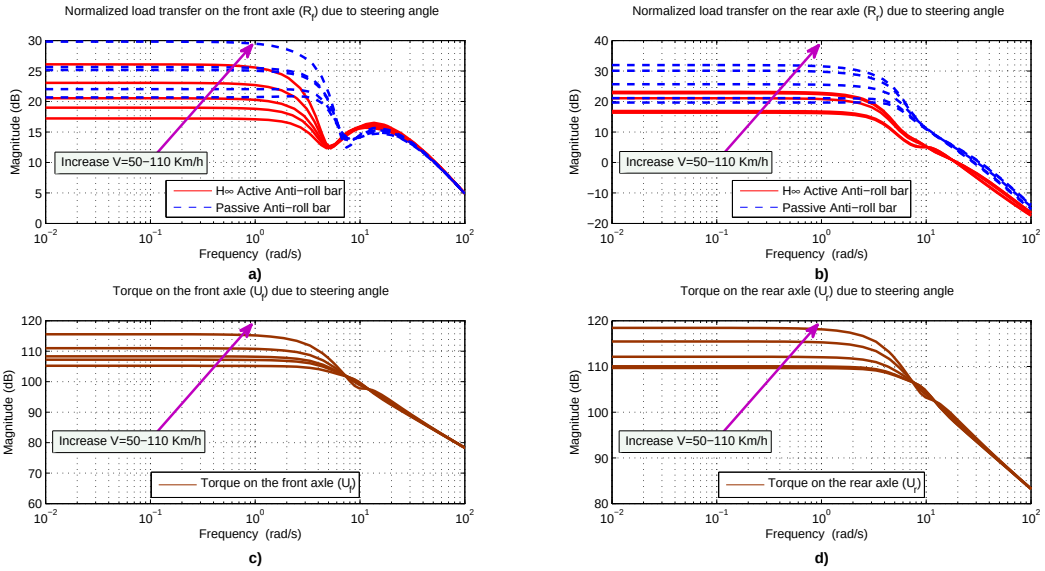

Fig. 11. Frequency responses of the normalized load transfer ($R_{f,r}$) and the torque ($U_{f,r}$) due to steering angle.

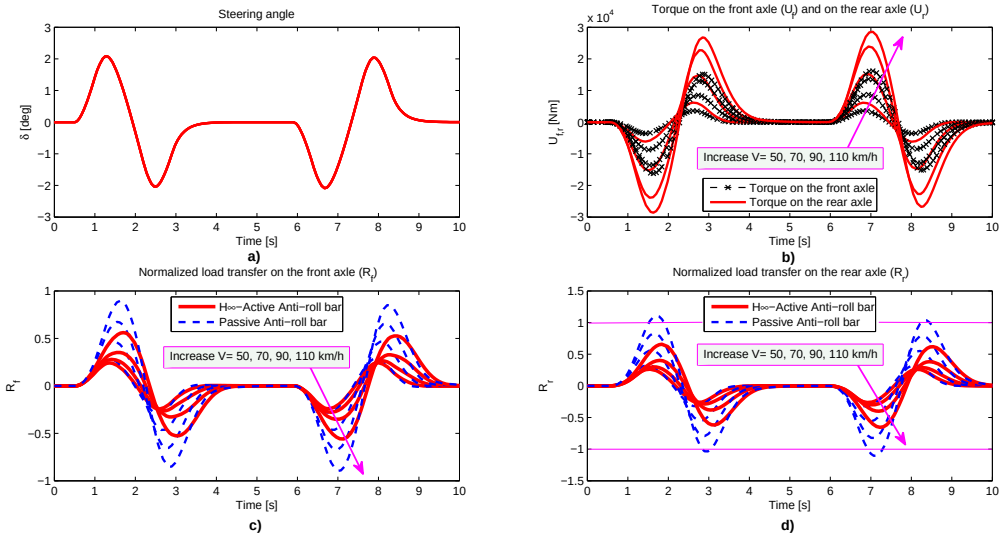

Fig. 12. Time responses of normalized load transfer and torque at the axles of single unit heavy vehicle.

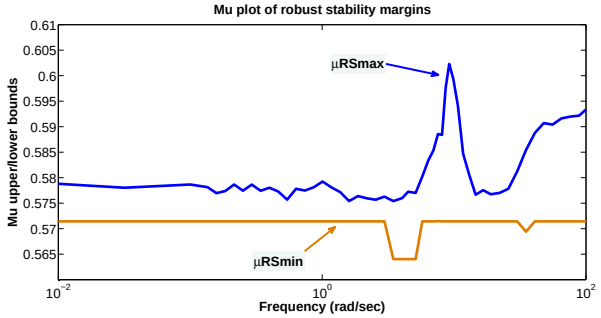

Fig. 9. Upper and Lower bounds for RS.

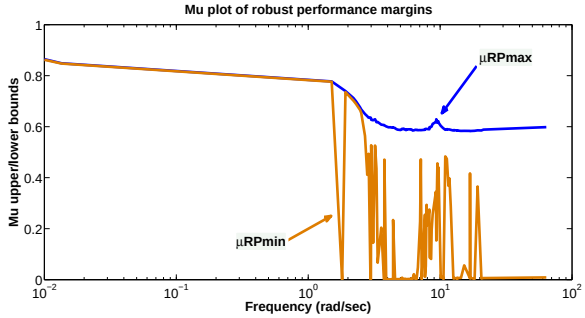

Fig. 10. Upper and Lower bounds for RP.

5.2 Effect of the forward velocity uncertainties on the closed-loop system behaviour

In this section, the robustness of the H_∞ active anti-roll bar control is evaluated by changing the forward velocity from $50Km/h$ to $110Km/h$.

Fig $11a,b$ show the normalized load transfer at the front axle R_f and at rear axle R_r due to steering angle δ_f with the forward velocity variation. When compared to the passive anti-roll bar, One sees that the normalized load transfers at the front axle R_f

in case of the H_∞ active anti-roll bar control have been reduced in frequency range up to $7.0 rad/s$. Meanwhile the normalized load transfers at the rear axle R_r have been reduced throughout the main frequency range. The reduction of the normalized load transfer at the front and at the rear axles in desired frequency range improves then the roll stability which prevents the rollover of the single unit heavy vehicle.
Fig 11c,d show the control inputs (U_f, U_r) of the H_∞ active anti-roll bar at two axle. The torque at the rear axle is always greater than that of front axle throughout the main of the frequency range when the forward velocity varies from $50 Km/h$ to $110 Km/h$.
From the simulation results above, we can claim that the H_∞ active anti-roll bar control is robust w.r.t. the forward velocity variation.

6. SIMULATIONS IN TIME DOMAIN

In this section, the considered vehicle maneuver is a double lane change for overtaking. The lane used to overtake another vehicle is almost always a passing lane further from the road shoulder. Figure 12a shows the steering angle δ corresponding to a double lane change. The forward velocity is considered constant from $50 Km/h$ to $110 Km/h$.
Fig 12c,d show the normalized load transfers at the front and rear axles, respectively. With the H_∞ active anti-roll bar, the values of normalized load transfer at the front and rear axles are always within ± 1, while the normalized load transfer at rear axle of the passive anti-roll bar exceeds ± 1 when the forward velocity $V = 110 Km/h$. At this velocity, the wheels of vehicle lift on, leading to rollover.
Fig 12b shows the torques at front and rear axles. They increase with the forward velocity.
Fig 13 summarizes the performance assessment of the roll stability of the single unit heavy vehicle using the H_∞ active anti-roll bar control. The *Root Mean Squares (RMS)* of the normalized load transfers and the roll angles of suspension are compared to that of the passive anti-roll bar (corresponding to 100%).

$$\frac{RMS(active)}{RMS(passive)} 100\% \tag{25}$$

The RMS of the H_∞ active anti-roll bar control have been reduced from 15% to 50% compared to the passive anti-roll bar. It also shows that the H_∞ active anti-roll bar control has reduced a lot of the RMS values when the forward velocity varies from $70 Km/h$ to $100 Km/h$. This is also the *"danger"* zone of the forward velocity of heavy vehicle when the vehicle maneuver is a double lane change to overtake.

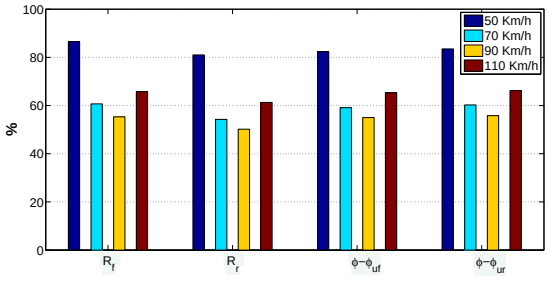

Fig. 13. RMS of the H_∞ active anti-roll bar control compared to the passive anti-roll bar (100%).

7. CONCLUSION

In this paper, the *Yaw - Roll* model of a single unit heavy vehicle including active anti-roll bar systems at two axles is used. A linear H_∞ control scheme is developed to maximize its roll stability in order to prevent rollover. The normalized load transfers and the limitations of the torque generated by actuators are considered.
Simulation results both in frequency and time domains demonstrate that the H_∞ active anti-roll bar control completely reduces the normalized load transfers and the roll angles of suspension compared to the passive anti-roll bar. A μ- analysis confirms that the closed-loop system remains stable for larger uncertainties with the forward velocity $V = 70 Km/h \pm 94.87\%$ and the sprung mass $m_s = 12487 kg \pm 49.81\%$.
Even if a *LTI* controller seems to performs reasonably well here, the comparison with an *LPV* controller (scheduled by the vehicle velocity) will be of interest.

REFERENCES

Bharane, P., Tanpure, K., Patil, A., and Kerkal, G. (2014). Design, analysis and optimization of anti-roll bar. *Journal of Engineering Research and Applications*, 4(9), 137–140.

Boada, M., Boada, B., Quesada, A., Gaucha, A., and Daz, V. (2007). Active roll control using reinforcement learning for a single unit heavy vehicle. In *12th IFToMM World Congress*. Besancon, France.

Gaspar, P., Bokor, J., and Szaszi, I. (2004). The design of a combined control structure to prevent the rollver of heavy vehicles. *European Journal of Control*, 10(2), 148–162.

Gaspar, P., Bokor, J., and Szaszi, I. (2005a). Reconfigurable control structure to prevent the rollover of heavy vehicles. *Control Engineering Practice*, 13(6), 699–711.

Gaspar, P., Szabo, Z., and Bokor, J. (2005b). Prediction based combined control to prevent the rollover of heavy vehicles. In *Proceedings of the 13th Mediterranean Conference on Control and Automation*. Limassol, Cyprus.

Sampson, D. and Cebon, D. (1998). An investigation of roll control system design for articulated heavy vehicles. In *4th International symposium on Advanced Vehicle Control, AVEC1998*. Nagoya, Japan.

Sampson, D. and Cebon, D. (2002). Achievable roll stability of heavy road vehicles. In *Proceedings of the Institution of Mechanical Engineers, Part D: Journal of Automobile Engineering*, volume 217. United Kingdom.

Sampson, D. and Cebon, D. (2003). Active roll control of single unit heavy road vehicles. *Vehicle System Dynamics: International Journal of Vehicle Mechanics and Mobility*, 40(4), 229–270.

Sampson, D.J.M. (2000). *Active Roll Control of Articulated Heavy Vehicles*. Ph.D. thesis, University of Cambridge, UK.

Scherer, C. and Weiland, S. (2005). Linear matrix inequalities in control. University Lecture.

Skogestad, S. and Postlethwaite, I. (2001). *Multivariable Feedback Control*. John Wiley & Sons, 2 edition.

Vu, V.T., Sename, O., Dugard, L., and Gaspar, P. (2016). Active anti-roll bar control using electronic servo-valve hydraulic damper on single unit heavy vehicle. In *IFAC Symposium on Advances in Automotive Control - 8^{th} AAC 2016*. Sweden.